CCIT Report #619, April 2007

Experimental validation of 20nm sensitivity of Singular Beam Microscopy

Boris Spektor, Alexander Normatov, Joseph Shamir
Electrical Engineering Department, Technion – Israeli Institute of Technology; Technion City, Haifa 32000, Israel;

ABSTRACT

Quickly developing nanotechnology drives the industrial need for fast but sensitive nano-scale feature detection and evaluation. In this work we bypass the diffraction limit for achieving nanoscale sensitivity by introducing optical singularities into the illuminating beam for a modified laser scanning microscopic architecture. A good correspondence was obtained between laboratory experiments and corresponding simulations that indicated a theoretical potential of 1nm sensitivity under a practical signal to noise ratio of 30dB. For analysis of the experimental and simulation results, two simple but effective algorithms were developed. A significant improvement of signal to noise ratio in the optical system with coherent light illumination can be achieved by utilization a highly redundant data collected during experiments. Our experimental results validate achievable sensitivity down to 20nm. The unique combination of nano-scale sensitivity together with implementation simplicity and on-line, real-time analysis capability make Singular Beam Microscopy a valuable industrial analytic method.

Keywords: Singular beam, nano-scale, microscopy, sensitivity

1. INTRODUCTION

Progress in high-tech production and scientific research relies heavily on high sensitivity instrumentation for measurements and quality control. Parameters to be evaluated include the dimensions and position of nano-scale surface features, surface roughness, surface defects and particle size distributions. High volume and high cost of production processes impose the need for high-sensitivity and high-speed inspection systems operating on the production lines.

Traditional approaches for high sensitivity surface inspection, such as confocal microscopy, scanning probe microscopy and interferometry cannot combine high speed with high sensitivity and spatial resolution, as required by cutting edge technologies. Singular Beam (SB) microscopy is being developed with an attempt to fill this technology gap.

As opposed to other techniques, that use Gaussian beam, plane wave or evanescent wave illumination, this method uses a singular beam. Based on the intensity pattern of a singular beam, scattered by the investigated surface, surface feature parameters can be deduced. While most of the other methods intend to generate images of investigated surface features, SB microscopy aims to collect more refined information. Generally, a singular beam contains one or more optical singularities, where the amplitude vanishes and the phase is indeterminate. At the early stages it became apparent that SB microscopy has nano-scale sensitivity[1-3]. In this paper we continue to investigate the capabilities of SB microscopy using a line phase singularity imbedded in a Gaussian laser beam. The principles of SB microscopy are provided in the next section and the experimental results are described in Sect. 3. This is followed by a discussion and conclusions.

2. SINGULAR BEAM MICROSCOPY

The main idea of the SB microscopy can be outlined as follows. A SB scans the investigated sample and interacts with objects, frequently of dimensions in the nanometer region. The light scattered from this interaction is propagated in free space and/or through optical systems and is recorded by a detection system and its intensity distribution is analyzed in time and space. The classical diffraction limit is evaded by collecting information as the object is scanned by the singular beam and the analysis of the scattered light is constrained by the overall system Signal-to-Noise Ratio (SNR), as opposed to the fundamental diffraction limit of conventional imaging systems.

2.1 Singular beams and their generation

A singular beam is a light beam that contains one or more optical singularities[3-6]. In this work we only deal with phase singularities that possess regions of indeterminate phase where the complex amplitude vanishes but other singularities, such as polarization singularities can also be considered. Although generally, SB microscopy deals with either one dimensional or two dimensional singularities, in this work we used a line phase dislocation as singularity. The line singularity was introduced in a Gaussian beam by means of a π phase step, which was fabricated by a special lithographic procedure and wet etching of glass substrate.

2.2 Singular beam microscope

The optical setup of a SB microscope used here for surface feature analysis is schematically presented in Fig. 1. A Gaussian laser beam is modulated by a mask with a π phase step that introduces the line phase dislocation and the SB is focused onto the focal plane of a microscope objective where it interacts with the investigated surface. Registration of the scattered beam intensity distribution is performed at the recording plane by a 6 Megapixel digital camera.

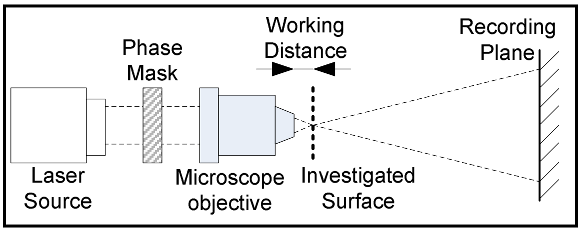

Fig. 1. Optical setup of the investigated SB microscope. A Gaussian laser beam passes through a phase mask that introduces optical singularity. The singular beam is focused onto the investigated surface and the light scattered is recorded with the digital camera.

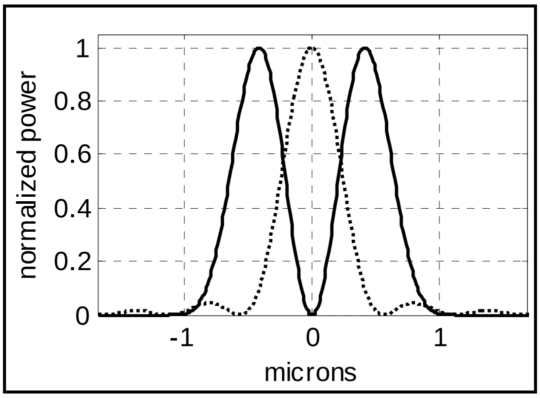

Fig. 2. An example of the SB intensity distribution (solid curve) vs. a corresponding Gaussian intensity distribution (dotted curve) at the focal plane of the microscope objective. The intensities are normalized to 1.

Fig. 2 presents a simulated intensity profile across a SB compared to the intensity profile of a corresponding Gaussian Beam (for numerical aperture of 0.4). Both intensity profiles are situated at the focal plane of the microscope objective. The phase dislocation causes the SB complex amplitude to be anti-symmetric leading to an absolute intensity zero at the center (where the amplitude crosses zero). The two intensity lobes of the SB can be viewed as two arms of an interferometer that can intuitively explain why nanoscale sensitivity is possible. For comparison of an experimental SB with a corresponding experimental Gaussian Beam at the recording plane see Fig. 3. Both the 2D images and profiles are provided.

3. EXPERIMENT

A series of experiments were performed to study the nano-scale sensitivity of SB microscopy at two different wavelengths (514 nm and 488 nm) of an Ar ion laser. Since similar results were obtained at both wavelengths we present here only the data obtained at 514 nm. All the experimental results are accompanied by simulations obtained by paraxial optics approximation in its operator representation[7].

3.1 Experimental setup

The experimental investigation was performed on an optical system shown schematically in Fig.1. Series of experiments were carried out, each possessing its own set of parameters, and the results were compared to corresponding simulations. The differences between experimental results and deviations from the simulated results are mainly attributed to imperfections in the optical system and the implementation of the π phase step. As a test object model, a 500 nm high phase step (PS) was lithographically prepared on a 1 mm thick glass substrate. This glass substrate was mounted on a nanopositioning stage with computer based motion control. It should be noted that the orientation of the test object PS is aligned in parallel to the PS that is imprinted on the phase mask used to generate the line phase dislocation singularity.

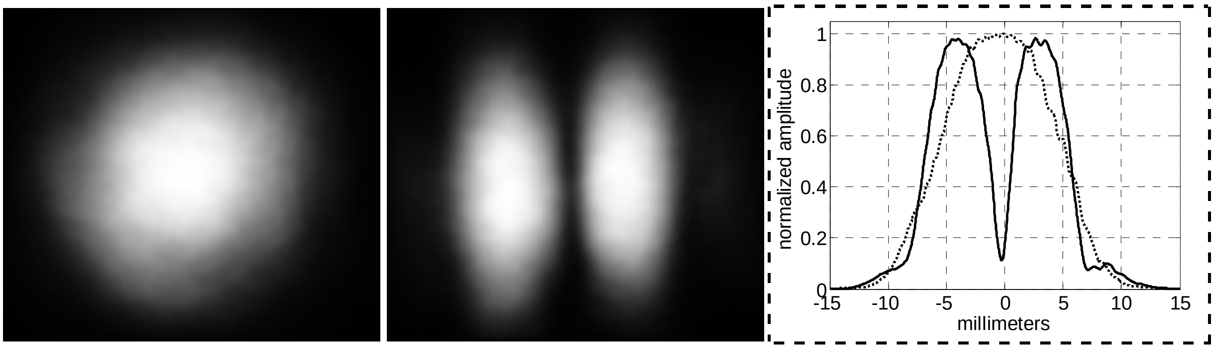

a. b. c.

Fig. 3. Experimental intensity distributions of the Gaussian beam (a) and SB (b), taken at the recording plane. Corresponding cross-section profiles (c) of Gaussian beam (dotted curve) and a SB (black curve).

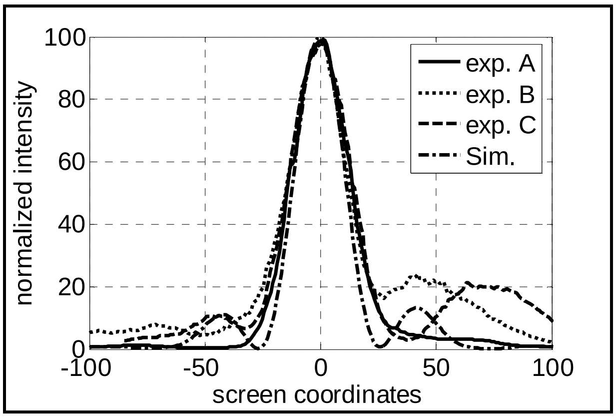

Fig. 4. Profiles of the intensity distribution in the recording plane. Semi dotted curve – simulation, other curves experiments. The phase step is situated at the center of the SB focal intensity distribution. Screen coordinates represent the recording plane.

The asymmetry of the side lobes of the experimentally obtained curves (A, B and C) in Fig.4 is caused by different surface roughness on the two sides of the π phase step edge (only one side was etched).

The experimental sensitivity was verified by nanoscale shifts of the PS (lateral position changes) relative to the SB focal intensity distribution. Although the shift value differed between the experiments, during a single experiment the shift value was kept constant (ranging from 20 nm to 50 nm). At each PS position (after each shift) scattered light distribution was recorded and compared to a corresponding simulation.

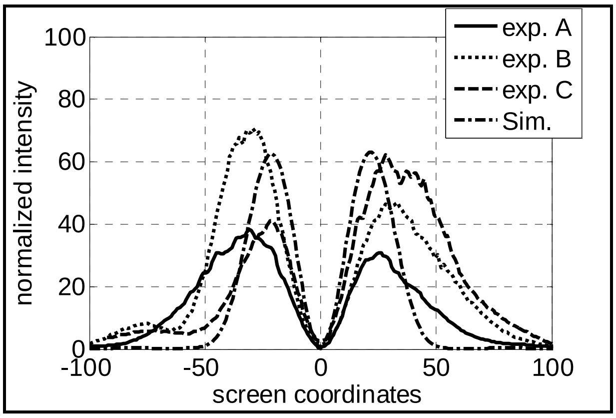

Fig. 5. Same as Fig. 4 but with the phase step situated outside the singular beam focal intensity distribution.

Figures 4 and 5 present simulation and experimental output intensity distribution profiles. Fig. 4 corresponds to the PS position at the SB focal intensity distribution center while Fig. 5 corresponds to the PS position at the external edge of the SB focal intensity distribution. In a typical experiment the PS scans through the whole singular beam focal intensity distribution leading to hundreds measurements in a single experiment. For example, 5 micrometers that are sampled with 25 nm shifts produce 200 measurements and the amount of data may reach 10 GB. Experimental curves are wider than the simulation due the imperfections in the optical setup. A sample selection of experimental measurements is shown in Fig. 6. The upper row shows the recorded 2D intensity and the bottom row shows the profile corresponding to the cross section marked in the upper row. The relative accuracy of each shift was of the order of 1 nm.

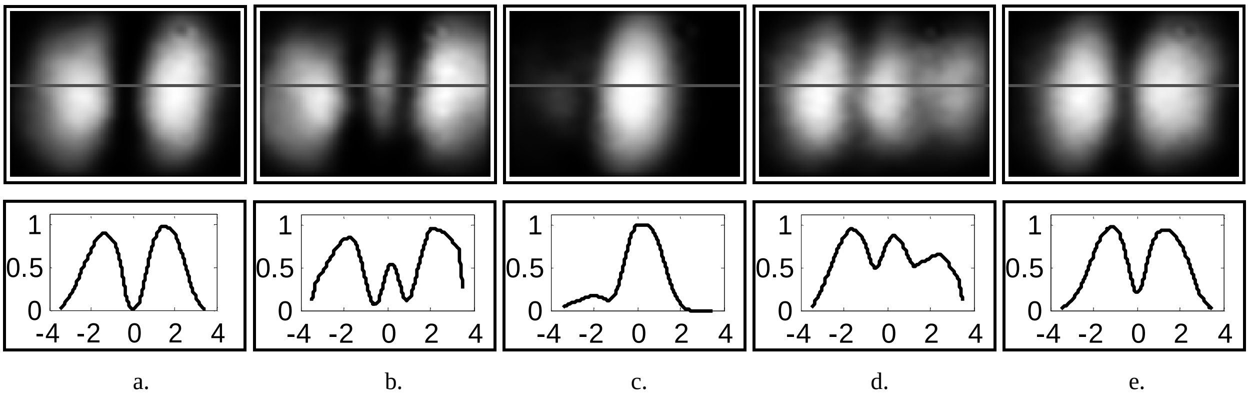

Fig. 6. Output intensity distribution (a)-(e) and corresponding profiles for the PS positions (shown from left to right): -4 µm, -2 µm, 0 µm, 1.8 µm, 4 µm. The vertical axis for pofiles is relative intensity.

3.2 Method of integration window analysis

Fig. 6 indicates that the central region of the output intensity distribution is most sensitive to a shift of the PS. Moreover, this region bears the most similarity to the simulations. Consequently, the simplest way of analysis of the experimental data would be to introduce an integration window, placed at the center of the output distribution, as shown in Fig. 7. The value of the total power in the window can be plotted against the PS position as shown in Figure 8. Although the experimental curves are wider (due to imperfections), the overall similarity between the nanoscale experiment and the simulation are apparent. Obviously, some optimization of the shape and position of the integration window can improve the results.

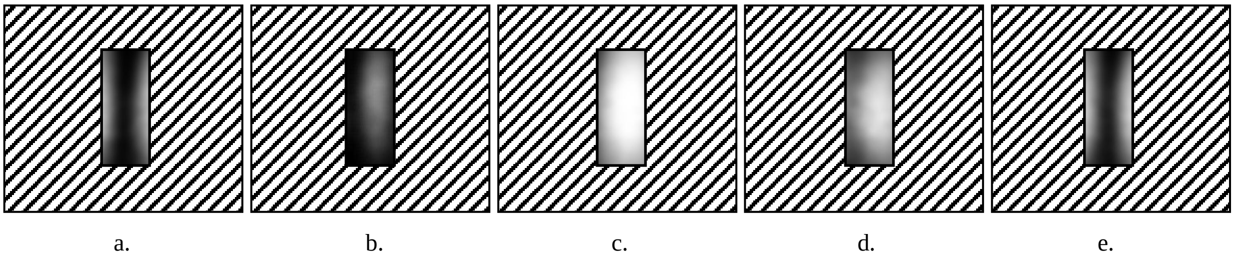

Fig. 7. Integration window application to output intensity distributions shown in Fig. 6. The integration (summation of intensity) is performed only on the pixels inside the window.

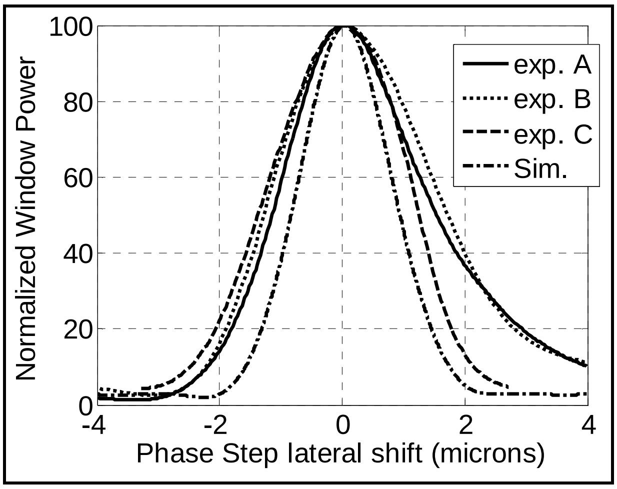

Fig. 8. Integration window power as a function of PS position. Vertical axis is relative power; horizontal axis is the PS position in microns. Semi dotted curve is simulation, other curves – experiments.

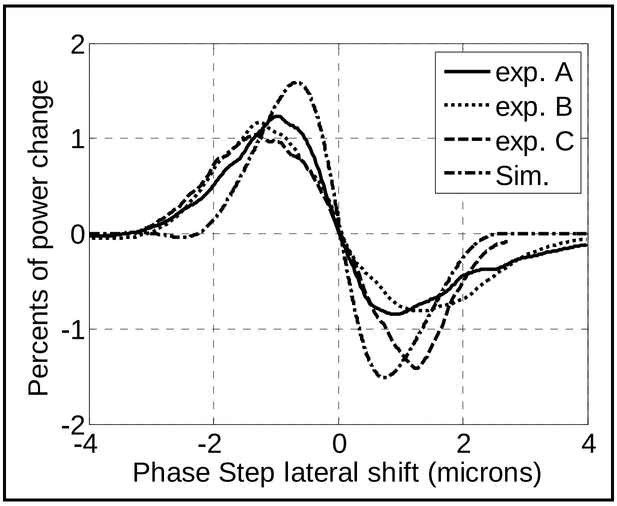

Fig. 9. Integration window power sensitivity as a function of PS position. The results are normalized to 20 nm PS shifts that were used in experiment C. Vertical axis is in percents of maximum integration window power; horizontal axis is PS position in microns. Semi dotted curve is simulation, other curves – experiments.

Based on the curves of Figure 8, the sensitivity achieved during the experiment can be evaluated. In this case the sensitivity can be defined as a relative change of output intensity distribution to a given change of PS position. In other words, it is a rate of change of window power as a function of position or, simply, a derivative of the curves in Fig. 8. This sensitivity is presented in Fig. 9. It should be noted that the sensitivity values of different experiments (that were performed with different PS shift values and different parts of PS edge) were normalized to the PS shift of 20 nm (as was the case in experiment C and the simulation).

The curves in Fig. 9 demonstrate a considerable similarity to the simulation, which is an important result for nanoscale shifts, measured using visible light. The values of an order of 1%, of maximum window power, for shifts of 20 nm can be discriminated and measured. This implies that such a simple optical setup, which includes technological imperfections of the elements, strongly demonstrates the ability of at least 20 nm shift sensitivity and can be implemented in fast real time applications.

3.3 Method of profile analysis

The method of integration window analysis described above is simple but it discards most of the available information. To exploit more information it is possible to utilize the whole output distributions shown in Figs. 4, 5 and 6. In this case it is convenient to leave the *x* axis as a screen (recording plane) coordinate and use the *y* axis for the PS position, relative to the singular beam focal intensity distribution. The profiles of consecutive measurements are placed one beside the other to form a profile map, as shown in Fig. 10 for simulation results and in Fig. 11 for experimental results corresponding to 20 nm PS shift.

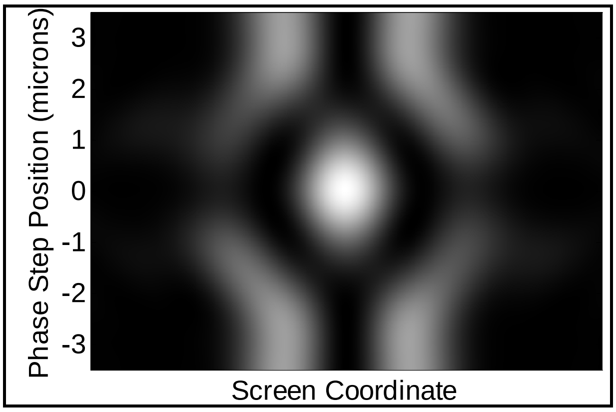

Fig. 10. Simulated output intensity distribution in the form of profile map. The result represents a simulation of an experiment with the PS scanning across the focal intensity distribution of the SB in shifts of 20 nm. For each position of the PS the intensity profile on the recording plane is coded in grayscale.

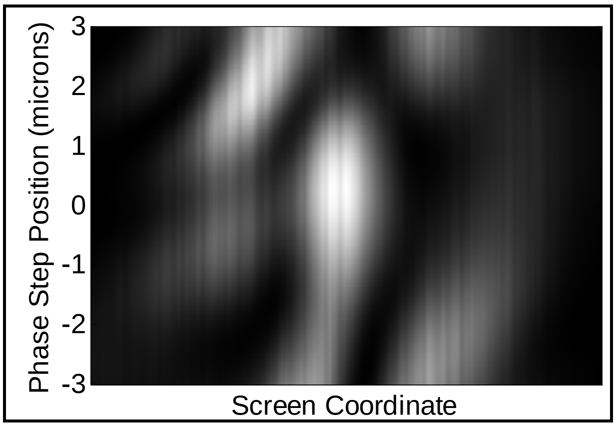

Fig. 11. Same as Fig. 8 but for experimental data.

Contrary to Integration Window analysis the profile analysis method uses less raw data in calculation of each point. Therefore the effects of speckle and interferences are more pronounced, such as the vertical lines imprinted on the intensity distribution seen in Fig. 11.

The sensitivity for the profile analysis can be calculated as a relative difference between output intensity profiles corresponding to adjacent PS positions. The sensitivity results corresponding to Figs. 10, 11 are shown in Figs. 12 and

13, respectively. Remarkably the sensitivity (in percents of the peak recording plane intensity) of the Profile analysis method is similar to that of the integration window analysis method and it is of an order of 1% of peak recording plane intensity for shifts of 20 nm.

As indicated above, the influence of optical system imperfections is enhanced and produces more distortions, especially when considering the sensitivity. A quick analysis of the simulation and experimental results proves that the selection of the central area for integration window analysis was justified both because the distortions there are much less pronounced than at the periphery and because the intensity changes (and consequently the sensitivity) are most prominent in the central region.

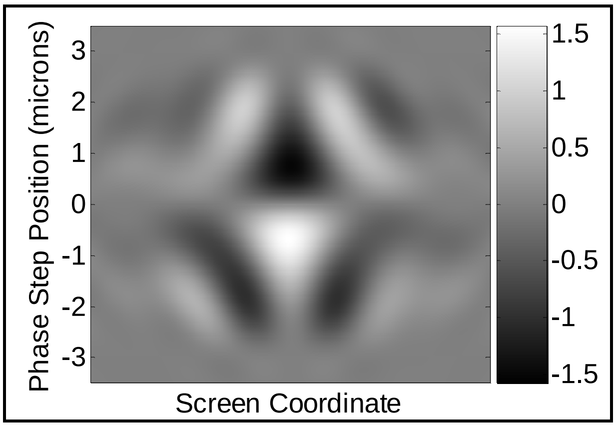

Fig. 12. Simulated sensitivity for the profile map of Fig. 11. The sensitivity result corresponds to a simulation of an experiment with the PS scanning across the focal intensity distribution of the SB in shifts of 20 nm. For each position of the PS the sensitivity profile is coded in grayscale.

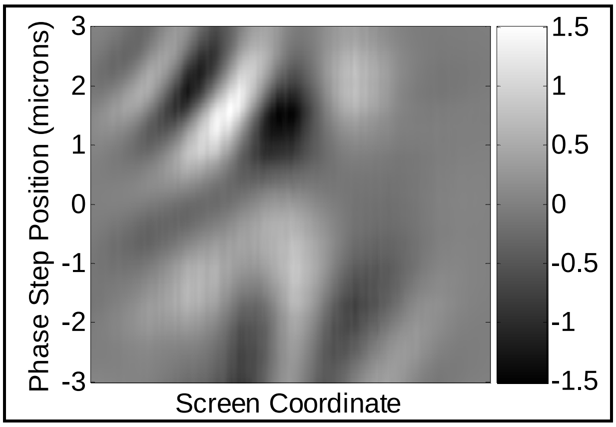

Fig. 13. As Fig. 12 but for the experimental sensitivity for the profile map of Fig. 11.

3.4 Analysis method considerations

The analysis methods described above represent a straightforward implementation. In the case of the integration window analysis method a single (scalar) value was used to characterize a given position of the PS. For the more sophisticated method of profile analysis each position of the PS is characterized by a profile (vector) and more advanced methods can be envisioned where a whole matrix is used for the position characterization.

A remarkable feature of both analysis methods is their ability to convert redundant information available from the measurement to improve the SNR. In the case of integration window analysis method a whole window is integrated into a single value thus effectively removing the adverse effect of both the speckle and interference. In the case of profile analysis method, data samples are integrated across the profile, thus reducing the effect of speckle, although in this case the number of integrated pixels is lower and consequently the noise and distortions are more pronounced.

In the examples treated in this work we restricted ourselves to the determination of a single feature parameter, the position of the PS. Obviously, other features, such as height, or a line width, can be evaluated as well. For such cases, the representation should deal with situations (rather than positions) represented by scalar, vector or matrix values. Clearly, when more information about a situation is available more features can be evaluated. On the other hand, extracting more information from a single measurement usually means fewer pixels integrated to obtain a value. This has an adverse effect on SNR. Therefore a specific analysis method should be carefully chosen according to the required application.

4. DISCUSSION

Using standard laboratory equipment the experimental results presented above demonstrated a sensitivity of 20 nm with a working distance 1 mm. Thus, SB microscopy enables nanoscale sensitivity at high scanning speed (as that of confocal microscopy). Moreover, the required numerical analysis is relatively simple and can be also handled at high speeds with conventional computing power. The description and results presented above show that in the case of SB microscopy the investigation sensitivity depends solely on SNR (rather than on diffraction limit, for instance). This means that the sensitivity can be improved by improving the SNR of an investigation system.

4.1 Capability simulations of SB microscopy

The experimental results presented above correspond to a specific laboratory system not optimized to the full potential of SB microscopy. For instance, the focal intensity distribution for an ideal case (of NA = 0.4), as shown in Fig. 2, is about three times narrower than the corresponding focal intensity distribution of the experimental SB obtained. Therefore additional simulations were performed to investigate the theoretical capabilities of SB microscopy.

The additional capability simulations assumed an ideal optical system with NA = 0.4 and SNR = 30dB (including the processing gain obtained by an analysis method). Similar to the experiments, these simulations used a phase step as an object model. The simulations checked two cases: phase step shift and phase step height changes. As it is demonstrated in Fig. 12, the sensitivity is not uniform across various PS positions. Similarly it is not uniform across various PS heights either. Consequently, a sensitivity cutoff value was chosen such that it will hold for approximately 80% of PS situations (positions in the case of PS lateral movement). This ensures that the following simulation results have practical, rather that purely theoretical meaning. The results are: 2.5 nm sensitivity for lateral PS shift and 1.25 nm sensitivity for PS height change.

4.2 Applications of SB microscopy and its limitations

Alongside clear advantages of SB microscopy for industrial applications there are also disadvantages and limitations. First of all, to choose the proper method of data analysis, SB microscopy requires *a priori* information about the investigated object. Although this limitation represents a major issue for general microscopy, it is not so important in industry, where the investigated object is usually known. The second limitation of SB microscopy is the fact that it extracts information about object features rather than its image. Therefore, SB microscopy is evaluated in terms of a sensitivity metric rather than resolution metric. Again, industry is usually much more interested in evaluating object/surface features than in visualizing them. Finally, at the current state of art SB microscopy is developed only for certain classes of isolated objects.

The unique combination of the capabilities of SB microscopy for high sensitivity and high speed evaluation makes it an attractive choice for industrial applications, in spite of inherent limitations. One of the possible applications is alignment, which can be derived straightforward from the experiment discussed above. The other likely application is surface defect detection which can also be easily implemented, by simple monitoring of the output intensity distribution. Other possible applications include on-line production control, particle sizing and lithographic photomask registration.

5. CONCLUSIONS

An experimental demonstration of the sensitivity of SB microscopy was presented along with numerical analysis. The principle of SB microscopy eliminates the classical diffraction limits that exist for conventional imaging systems, trading it off with limitations imposed by the overall SNR of the system and the requirement for some *a priori knowledge*. Paraxial simulation of an ideal case predicted sensitivity comparable to modern interferometric methods under reasonable SNR assumption. Analysis of experimental results confirms sensitivity of 20 nm with a potential of improvement by at least an order of magnitude. Such high sensitivity combined with high scanning speed that is due to sufficiently long working distance makes SB microscopy an attractive tool for industrial applications.

Acknowledgements

This work was performed within the NANOPRIM project supported by the European Community under the FP6 program. B. Spektor was also partially supported by the Center for Absorption in Science, Ministry of Immigrant Absorption, State of Israel.

REFERENCES

1. B. Spektor, G. Toker, J. Shamir, M. Friedman, A. Brunfeld, "High resolution surface feature evaluation using multi-wavelength optical transforms", *in Interferometry XI: Techniques and Analysis*, SPIE Proc. 4777, 345-351 (2002).
2. G. Toker, A. Brunfeld, J. Shamir, B. Spektor, E. Cromwell, J. Adam, "In-line optical surface roughness determination by laser scanning", *in Interferometry XI: Techniques and Analysis*, SPIE Proc. 4777, 323-329 (2002).
3. A. Tavrov, N. Kerwien, R. Berger, H. Tiziani, M. Totzek, B. Spektor, J. Shamir, G. Toker and A. Brunfeld, "Vector simulations of dark beam interaction with nano-scale surface features", *in Optical Measurement Systems for Industrial Inspection III*, SPIE Proc. 5144, 26-36 (2003).
4. J. F. Nye and M. V. Berry, "Dislocations in Wave Trains", Proc. R. Soc. Lond. A. **336**, 165-190 (1974).
5. I.V. Basistiy, MS. Soskin, M.V. Vasnetsov, "Optical wavefront dislocations and their properties", Optics Communications **119**, 604-612 (1995).
6. B. Spektor R. Piestun, and J. Shamir, "Dark Beams with a constant notch", Opt. Letters **21**, 456-458 (1996).
7. J. Shamir, *Optical Systems and Processes*, SPIE Press, Bellingham, 1999.